International Journal of Multiphase Flow 159 (2023) 104321

Contents lists available at ScienceDirect

International Journal of Multiphase Flow

journal homepage: www.elsevier.com/locate/ijmulflow

Hydrodynamic forces in a horizontal-horizontal elbow in a gas-liquid system

C. Garcia [a,*], R. Nemoto [c], E. Pereyra [a], L. Korelstein [b], C. Sarica [a]

[a] McDougall School of Petroleum Engineering, The University of Tulsa, Tulsa, OK 74104, United States
[b] Piping Systems Research & Engineering Co, Russia
[c] TechnipFMC, FMC Kongsberg Subsea AS, Norway

ARTICLE INFO

Keywords:
Hydrodynamic force
Flow-induced force
Flow-induced vibration
Multiphase flow
Flow pattern
Slug
Pseudo-slug
Flow density
Flow velocity
Flow frequency

ABSTRACT

Understanding the force fluctuations in an elbow is critical for piping system design, especially in multiphase flow applications. A new experimental facility has been designed and built where flow parameters, structural forces, and pressure upstream and downstream of the elbow can be measured simultaneously. The new facility allowed the study of the impact of different flow patterns on the phenomenon, with a wide range of liquid and gas superficial velocities (v_{SL} 0.1-2.5 m/s, v_{SG} 1-10 m/s). Oil and air have been used to represent field conditions better. In-situ liquid holdup and structure or translational velocity instead of mixture velocity are characterized. The flow influence as the peak force magnitude was measured on a single elbow (90-degree) oriented in a horizontal-horizontal configuration to identify the flow parameters with the most effect on the force. The results show that the density and velocity of coherent flow structures are essential to describe the force fluctuation. Additionally, pressure fluctuations in the elbow are significant for estimating the force in specific flow patterns.

1. Introduction

Intermittent flow, such as slug flow, prevails in the transport of liquid and gas in a pipe, where the velocity and density of fluid structures change over time, inducing cyclic stresses in the pipe. For slug flow, typically, the frequencies are 0.02-10 Hz. Therefore, the frequency of these flow stress cycles could be in the thousands or tens of thousands per hour, equivalent to millions of stress cycles per year. Understanding the nature of these cyclic stresses is vital in determining the fatigue life of a piping system. Thus, when design codes are used to define the fatigue life of these systems (i.e., DNV-05-F101, 2013 or ISO 14692), it is possible to determine the magnitude of the allowable stress (S) as a function of the number of cycles (N). This is done using S-N diagrams (i.e., BS 7608:2014+A1:2015, for steel products). Thus, two critical parameters to determine the fatigue of piping systems due to multiphase flow are a) the range of stress or the magnitude of the force peaks caused by the impact of such structures on the accessories (i.e., elbows) and b) the frequency of fluid structures with higher density and velocity (i.e., slug bodies).

Most of the previous studies of flow-induced vibration (FIV) for internal two-phase flow in piping systems have some commonalities. The experimentation includes the change of mixture velocity and volumetric quality (gas void fraction) for a given pressure and temperature. Most studies have used water and air as fluids. The main differences are the flow direction, type of fitting, type of sensor to measure the structural response, and the nature of multiphase flow characterization. A bend was studied using force sensors for horizontal direction by modifying water surface tension and viscosity, including conductance probes for slug flow characterization (Tay and Thorpe, 2004). Bends and T-joint were investigated using pressure, force, and optical sensors for flow characterization and to determine the amplitude and frequency of force pulsations (Belfroid et al., 2010, Cargnelutti et al., 2010). A single bend and large structures with multiple bends were investigated using cameras and tomography to measure multiphase flow behavior (Belfroid et al., 2016). Vibration for two different span distances was tested in a clamped-clamped horizontal PVC pipe (Ortiz-Vidal et al., 2017). Wang et al. (2018) investigated the transversal displacement in a horizontal pipe, where the two-phase flow parameters were obtained using differential pressure transducers.

Previous studies identified recurring remarks from the investigation of FIV in two-phase flow: (a) the maximum magnitudes of the induced forces are observed in the slug flow pattern or slug-annular transition, (b) the amplitude of the force increases predominantly with the flow velocity in intermittent flow, and (c) the predominant vibration frequency increases with increasing liquid fraction for a given an average

* Corresponding author.
E-mail address: ceg9863@utulsa.edu (C. Garcia).

https://doi.org/10.1016/j.ijmultiphaseflow.2022.104321
Received 28 July 2022; Received in revised form 21 October 2022; Accepted 13 November 2022
Available online 15 November 2022

Nomenclature

PSD	power spectral density
DFT	discrete Fourier transformation
d	pipe diameter, m
μ_S	slug viscosity, Pa.s
H_L	in-situ liquid holdup
v_T	structure velocity, m/s
v_M	mixture velocity, m/s
v_{SL}	liquid superficial velocity, m/s
v_{SG}	gas superficial velocity, m/s
H_{LLS}	slug liquid holdup
ρ_s	structure density, kg/m3
A	pipe cross-sectional area, m2
F_x	X-direction overall force, N
F_y	Y-direction overall force, N
H_{LM}	in-situ average liquid holdup
F_R	resultant force, N
F_H	hydrodynamic force, N
P_E	elbow pressure, psig
F_{Hs}	expected hydrodynamic force, N
F_{range}	expected force magnitude, N

flow velocity (Yih and Griffith, 1968).

No significant effects on the forces are observed when water surface tension is reduced by 32% or when water viscosity is increased by a factor of 2.62 (Tay and Thorpe, 2004). For a given void fraction and flow velocity, forces on bends and a tee are similar (Riverin et al., 2006). There appears to be no significant effect of the radius of curvature of the tested elbows on the excitation forces (Riverin and Pettigrew, 2007; Belfroid et al., 2010). However, pressure and gravity might enhance the force fluctuations caused by momentum flux (ρv^2), the leading cause is the impact force between the fluid structures of the liquid phase and the elbow (Liu et al., 2012). With regards to a single bend versus U-bend structures, no change in force dynamics on the downstream elbows is observed; the amplitude is very similar between both elbows, but the U-bend does introduce significant changes to the flow structures and, therefore, to the amplitude forces (Belfroid et al., 2016). Finally, the two-phase damping can be responsible for a lower force response in dispersed flow being similar to single-phase excitation (Ortiz-Vidal et al., 2017)

The reviewed literature shows that FIV is related to hydrodynamic behaviors of two-phase flow. Thus, by using comprehensive mechanistic models of liquid-gas flow, it is possible to predict better flow patterns, flow structure velocity (or translational velocity for slug flow), liquid holdup, pressure gradients (for slug and film regions), and other flow characteristics (Zhang et al., 2003). The present study covers essential aspects to facilitate the application of mechanistic models of gas-liquid pipe flows in the analysis of fatigue of piping systems due to multiphase flow.

In this study, we used oil with a density of 800 kg/m^3 and a viscosity of 6 cp at 80°F as a liquid phase instead of water to better represent field conditions. We monitored the in-situ liquid holdup to understand further the influence of fluid dynamics on the cyclic forces and used structure or translational velocity instead of mixture velocity. The peak force magnitudes were measured on a single elbow to identify the flow parameters with the most effect on the force. The intermittent flow and the predominant vibration force measured frequencies were compared. Moreover, time signatures of the upstream liquid holdup, upstream pressure, downstream pressure, and structural reaction force were synchronized to evaluate the influence of local pressure fluctuations on the force magnitude.

2. Experimental setup

This section describes the experimental facility and the instrumentation utilized in the study.

2.1. Multiphase characterization loop

The 50.8-mm ID horizontal oil/gas two-phase experimental flow loop of Tulsa University Fluid Flow Projects (TUFFP) is used in this study (see schematic in Fig. 1). The facility has an oil transfer tank, progressive cavity pump (20-hp screw pump), oil heater (20-kW Chromalox, 21-60°C), gas (air) delivering system (20-hp Gardner Denver dry rotary screw-type compressor, 1030 CFM at 100 psig), Y-2 type liquid/gas mixing tee (gas flows through thin pipes to avoid the formation of premature slugs), and 18.9-m long clear PVC pipe.

The instrumentation includes Micro-Motion mass flow meters, capacitance probes (CP, two-wire type), resistance temperature detectors, pressure transducers, and differential pressure sensors. One pair of CP (CP1 and CP2) is used to analyze the slug characteristics, such as the slug length, frequency, and translational velocity. High-quality

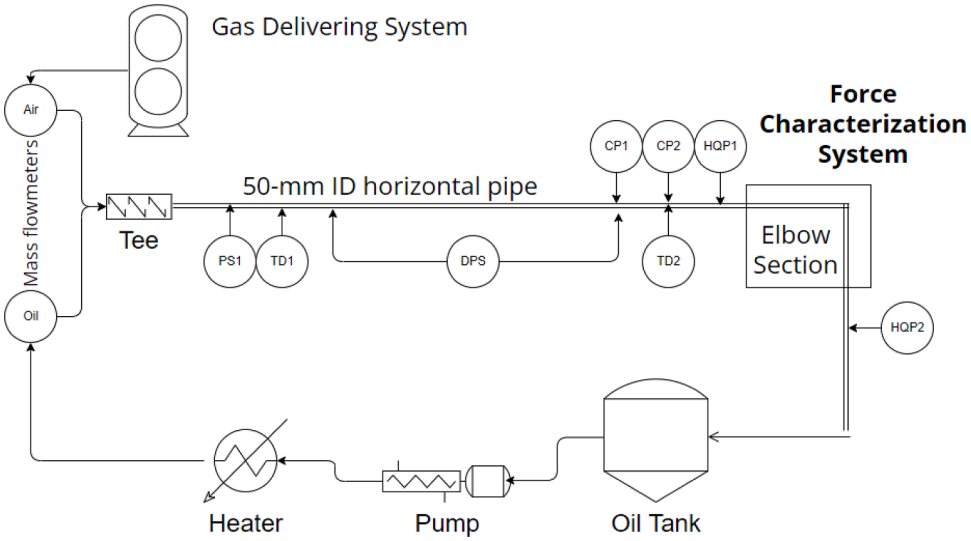

Fig. 1. Schematic of the experimental facility.

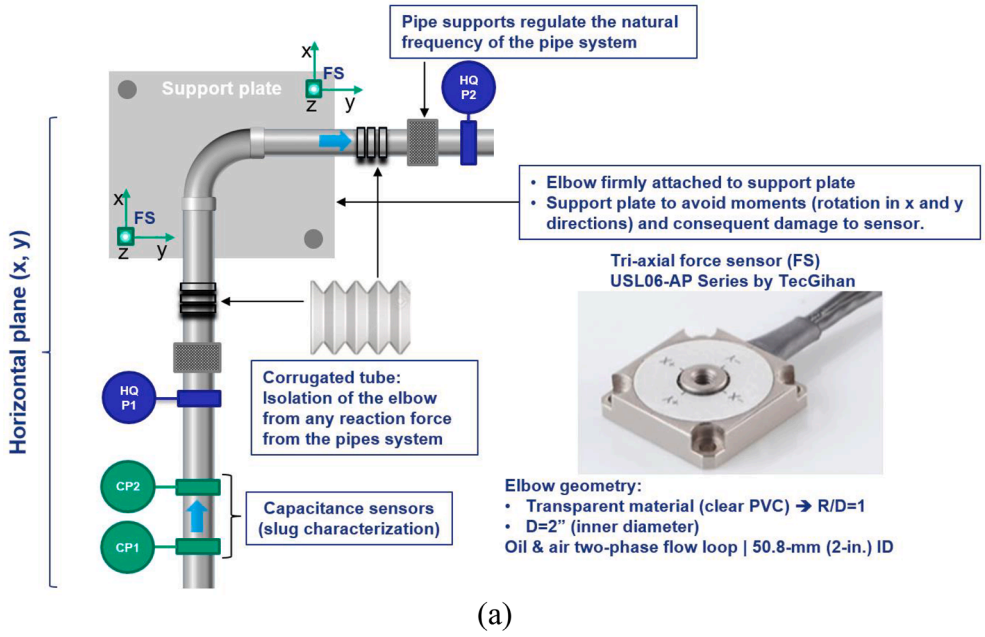

Fig. 2. TUFFP-FIV System: (a) instrumentation, (b) perspective and sensor distance.

pressure sensors (HQP) are installed to evaluate the pressure influence on the force elbow system.

The force characterization system is installed to evaluate FIV on a horizontal elbow at the end of the straight horizontal pipe. After the test elbow, there is a return line until the oil tank with a length of around 25 m. The following section describes the system.

2.2. Force characterization system

Fig. 2 shows a schematic of the force characterization system. The elbow section comprises two pieces of clear PVC pipes (50.8-mm ID, 0.5 m long) connected to a 90° transparent elbow (radius 50.8 mm, R/D=1.5). The elbow section is loosely attached to the upstream and downstream piping by two 0.1 m long flexible corrugated pipes. The corrugated pipes allow the measurement of the hydrodynamic force without the influence of the piping structure. Although the corrugated tubes introduce a small force as a function of system pressure, this contribution is determined with single-phase dynamic tests. It is discounted during the multiphase flow tests. The force system is calibrated using static loading with different known weights in the X and Y directions.

The elbow is fixed to the upper surface of a thin metal plate. Two triaxial dynamic force sensors (TecGihan USL06-H5-500N) are installed diagonally under the thin plate. Two smooth rollers are installed under the thin plate on the other two sides to allow the plate to move freely. The elbow section is fixed at a 0.6 m x 0.6 m support table. The input flow direction to the elbow was used as X-axis on the force sensors, and the output flow direction from the elbow was Y-axis on the force sensors. The axial readings of the sensors are combined to obtain the total X and Y force values.

2.3. Fast response pressure sensors

Two high-quality pressure sensors (HQP1 and HQP2) are installed before and after the elbow to obtain high-speed pressure data and characterize the hydrodynamic peak force by subtracting the pressure

Table 1
Properties of mineral oil.

Viscosity, μ_L	Density, ρ_L	Surface tension, σ	Color
(Pa•s)	(kg/m^3)	(N/m)	(-)
6.2 @ 80°F	798 @ 80°F	0.023	Light yellow

force from the overall force measurements and evaluate the influence of pressure variation $\Delta P(t)$ on the magnitude of FIV under the elbow. The HQP transducers are located symmetrically at 0.95 m from the elbow.

2.4. Capacitance sensors

Two capacitance sensors, based on the dielectric constants of air and oil, are installed before the elbow to measure in-situ liquid holdup and the velocity of flow structures. The sensors have been calibrated using the procedure proposed by Brito (2012). A calibration curve is built using a set of quick-closing valves. The calibration curve is utilized to convert dimensionless voltages into liquid holdup values.

2.5. Other instrumentation and data acquisition system

During the experiments, a data acquisition system monitors pressure, temperature, flow rates, output voltage from capacitance sensors, and mass gas and liquid flow rates. This system consists of a PC, a multi-function I/O board, and the LabVIEW™ software package. The output voltage from the force sensors is acquired with another data acquisition system, including a laptop, an amplifier, and the LabVIEW™ software package. All data files have TDMS format with a total test time of at least 1 minute. The high-speed data acquisition system has a rate of 1000 samples per second. Instrument systematic uncertainties are included for flow rates, densities, temperature, and pressure.

2.6. Fluid and operational conditions

Low-viscosity mineral oil was used during the experiments as the liquid phase. The oil has a light yellow color, and its viscosity and density were characterized using a dynamic rheometer and single-phase oil runs in the facility and are presented in Table 1 at 80°F. The viscosity and density are correlated for flow analysis following recommended practices (ASTM D341-09, 2015; Gottfried, 1965)

A flow pattern map was generated for the fluid properties and pipe geometry using the Barnea model for predicting flow-pattern transitions (Barnea, 1987). A wide range of liquid and gas superficial velocities were studied (v_{SL} 0.1-2.5 m/s, v_{SG} 1-10 m/s) The following flow patterns were obtained by varying the gas and liquid superficial velocities: slug flow (SL, 54 data points), pseudo-slug (PSL, 20 data points), and annular flow (ANN or A, 9 data points). Additionally, the transitions to dispersed bubble (DB, 3 data points) and stratified (ST or SS, 6 data points) are identified (see the experimental test matrix in Fig. 3). The system has limitations in exploring additional flow conditions due to the pipe design pressure of 15 psig dictated by the acrylic material. All the test points were repeated three times to check the precision of the measurements.

3. Experimental results

The total magnitude of the force peaks was studied; by subtracting the time-variant pressure-induced force from the total force, which is the hydrodynamic force or momentum flux (ρv^2).

The data collected from the experimental facility is processed using two main steps (see Fig. 4). First, signal processing obtains structure (translational) flow velocity and peak force parameters (frequency and magnitude) acting on the elbow. Second, density characterization provides the in-situ liquid holdup and the density of the structures (slugs, pseudo-slugs, or waves) hitting the elbow.

This data analysis provides the input variables to calculate the hydrodynamic force related to the force peaks' magnitude. The results are compared with force measurements to identify the most relevant variables.

Errors exist in every measurement. Uncertainty analysis provides confidence in the quality of the experimental data (Dieck, 2007). This analysis includes the estimation of the combined random and systematic uncertainties for recorded parameters (pressure, temperature, mass flow rates) and the estimation of uncertainty propagation on study variables (liquid density, gas density, superficial liquid velocity, superficial gas velocity, and mixture velocity). The used uncertainty models are explained in Brito (2012). The uncertainty propagated is lower than 2% for all the study variables.

Next are the results ordered in two parts: (1) multiphase flow characterization to validate the flow pattern influence on flow structure velocity, structure density, hydrodynamic force, and frequency of flow

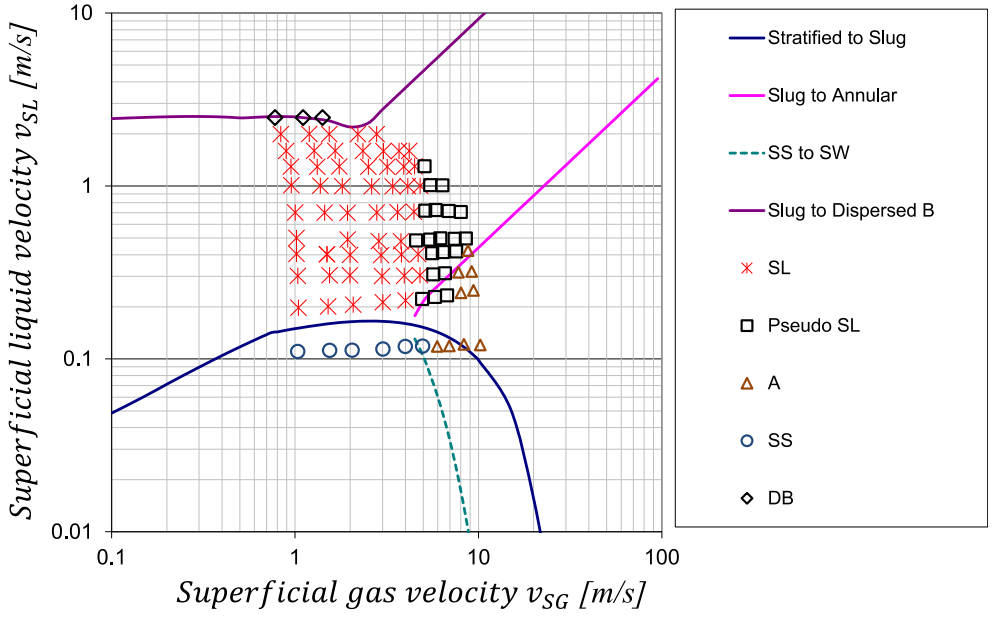

Fig. 3. Experimentally observed flow patterns on top of Barnea's (1987) map.

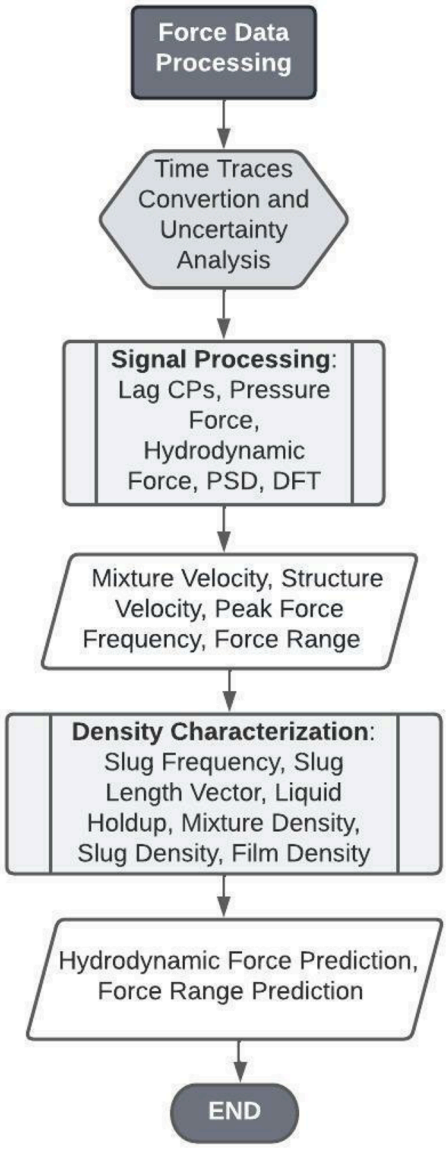

Fig. 4. Data Processing Flow Chart.

structures, and (2) flow structure signal synchronization with force signatures to identify the influence of pressure fluctuation on the magnitude of the force peaks.

3.1. Flow pattern influence

The characterization of flow structures as slugs, pseudo-slugs, or waves is done by monitoring the in-situ liquid holdup (H_L), using the capacitance probes. These flow structures move at velocity (v_T) which is measured by determining the time delay between two consecutive CP sensors (in milliseconds). Fig. 5 shows a data sample (time interval between 30.000 - 35.000 milliseconds) of a flow structure monitored with the CP sensors for slug flow.

Fig. 6 shows the flow structure velocity measurements for all the experimental repetitions. The data point values represent the mean for the repetitions, and the error bars its standard deviation. For low v_{SL} values (0.1, and 0.2 m/s), there are some conditions with moderate variation (high standard deviation between repetitions). On the other conditions with less variation ($v_{SL} \geq$0.3 m/s), the structure velocity increase linearly with a characteristic slope with the increase of mixture velocity. This slope is reduced for a mixture velocity of around 5 m/s.

The evaluation of the structure velocity is essential to identify the transition between the slug, pseudo-slug, and wavy annular flow patterns. For a slug, the translational velocity (v_T) is the sum of the drift velocity (v_D), which is the velocity of a Taylor bubble in a stagnant liquid, plus the contribution of the mixture velocity (v_M) in the preceding slug as:

$$\boldsymbol{v_T = C_o v_M + v_D}, \tag{1}$$

where C_o is a flow distribution coefficient that is approximately 1.2 for turbulent flow and 2.0 for laminar flow, based on the slug-body Reynolds number ($(\rho_S d v_m)/\mu_S$).

The translational velocity is linearly dependent on the mixture velocity for slug flow; thus, for a given superficial liquid velocity (v_{SL}), by increasing the superficial gas velocity (v_{SG}), and consequently the mixture velocity ($v_M = v_{SL} + v_{SG}$), the translational velocity will increase proportionally (Shoham, 2006). However, as the gas flow rate increases, the flow pattern changes from slug to pseudo slug. This flow pattern involves a continuous gas passage through the slug body. Pseudo slug (PSL) is described as the transition between the conventional slug (SL) and segregated flows (stratified and annular) in horizontal or slightly inclined pipes (0° to 30° from horizontal). It could be modeled as a segregated flow with very large waves, altering the gas and liquid momentum exchange (Soedarmo, 2018).

PSLs exhibit lower flow structure velocity than the expected linear increase for SLs. Fig. 6 shows the results of the flow pattern characterization using the evaluation of the flow structure velocity. For wavy annular flow (ANN) at low liquid (v_{SL}<0.2 m/s) and high gas flow rates (v_{SG}>7.0 m/s), the liquid film thickness is low, and liquid is swept up and around the pipe, creating a liquid-film annulus. Therefore, PSL is validated as a transition between SL and ANN. Finally, at v_{SL}=0.1 m/s, the flow is stratified (ST) with some waves moving at low velocities.

The liquid holdup and the structure density can be obtained from the monitoring of dimensionless voltage ($V^{'}$) using the CPs. With this information and using the oil and gas densities, it is possible to calculate the density in the slug bodies or large waves with high average holdup values. For slug flow pattern, the structure density includes the slug body holdup (H_{LLS}) as follow:

$$\boldsymbol{\rho_s = \rho_L H_{LLS} + \rho_G (1 - H_{LLS})}. \tag{2}$$

Fig. 7 shows the results of the flow pattern characterization using the evaluation of the slug/pseudo-slug/wave densities. The influence of flow pattern on the structure density follows two trends depending if the flow is intermittent (SL) or separated (ST, ANN). High values of density (450-750 kg/m3) represent slug flow conditions, and low values of density (<200 kg/m3) represent stratified wavy and annular wavy conditions when the mixture velocity goes to high values (v_M>4 m/s). The main observation is that PSL structure densities are between those two trends, with moderate values (150-550 kg/m3). The calculated structure density could be predicted using a well know model for the estimate of H_{LLS} for horizontal gas-liquid slug flow and is included as a reference (Gregory, 1978),

$$\boldsymbol{H_{LLS}} = \frac{1}{1 + \left(\frac{v_M}{8.66}\right)^{1.39}}. \tag{3}$$

On the other hand, the multiphase flow characterization to validate the flow pattern influence on hydrodynamic force is done by subtracting the effect of the time-variant pressure. As is mentioned in Belfroid (2016 b), "the force in a 90° bend is given by a pressure and momentum effect (with A, the cross-sectional pipe area) […]. For the transient analysis, we take the transient pressure and density". For each direction, the force is given by:

$$\begin{aligned} F_x(t) &= \left[P_1(t) + \rho v^2(t)\right] A, \\ F_y(t) &= \left[P_2(t) + \rho v^2(t)\right] A \end{aligned} \tag{4}$$

The quantity related to the hydrodynamic force ($\rho_{(t)} v^2_{(t)} A$) can be

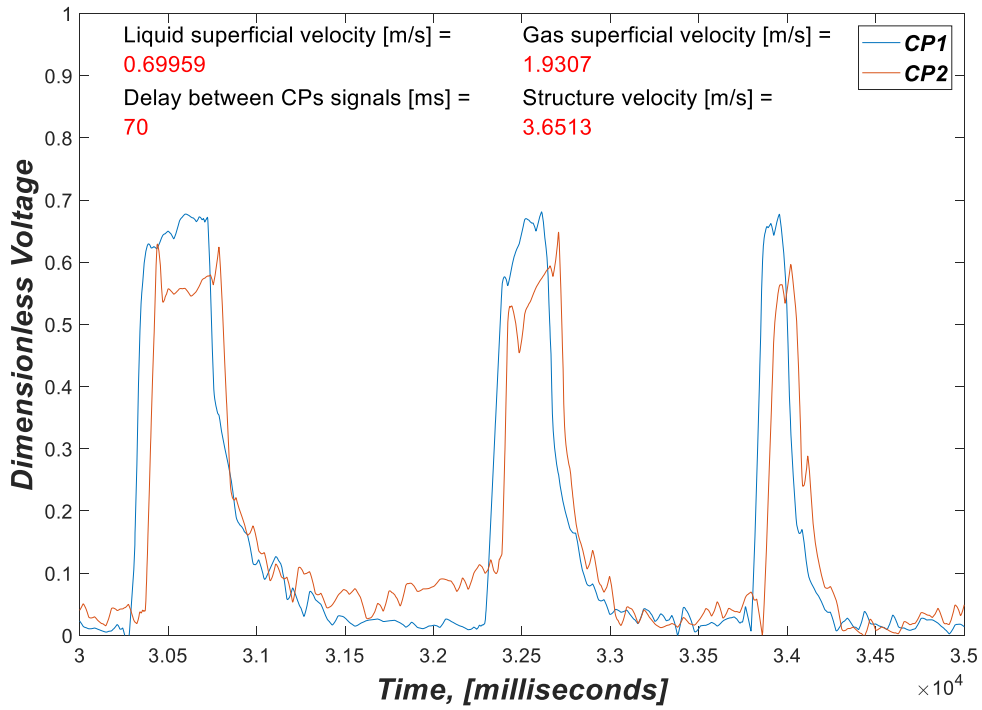

Fig. 5. Sample of slug flow structure monitoring ($\Delta t = 5\ s$).

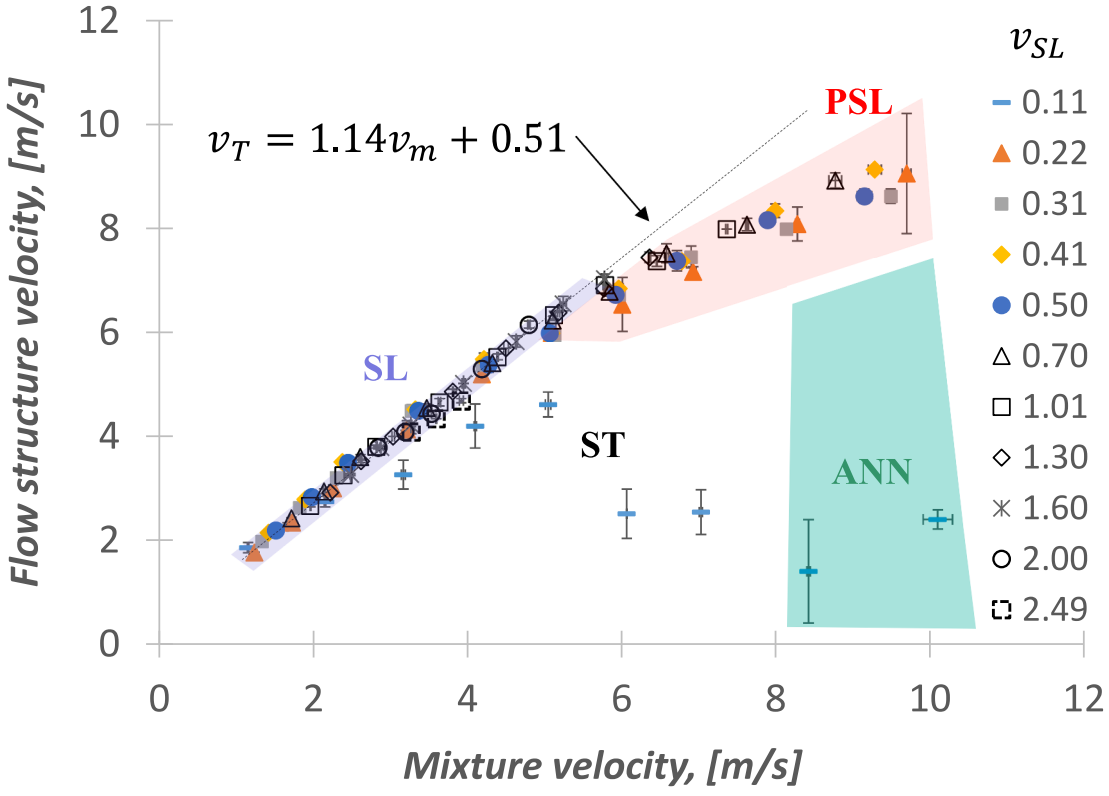

Fig. 6. Flow structure velocity (v_T).

obtained from the overall force and pressure measured on each side of the elbow. Fig. 8 shows a sample of force and pressure monitoring to characterize the hydrodynamic force. The pressure force to be subtracted is equal to the pressure times area ($(P(t)A)$), with pipe area $A = 0.00203\ m^2$. Figs. 9–12

Figs. 9 to 13 show the hydrodynamic forces (F_{HX}, and F_{HY}) for different gas flow rates (v_{SG}=1.93, 3.62, 5.13, 6.89, and 8.03 m/s), and for the same liquid flow rate (v_{SL}=0.70 m/s). For each condition, the time of capacitance data (CP1) is shifted to synchronize the flow structure with the force monitoring. This is done using the distance between sensors (3.27 m) and the structure velocity, and this synchronization facilitates visualization of the influence of dynamic forces in a horizontal

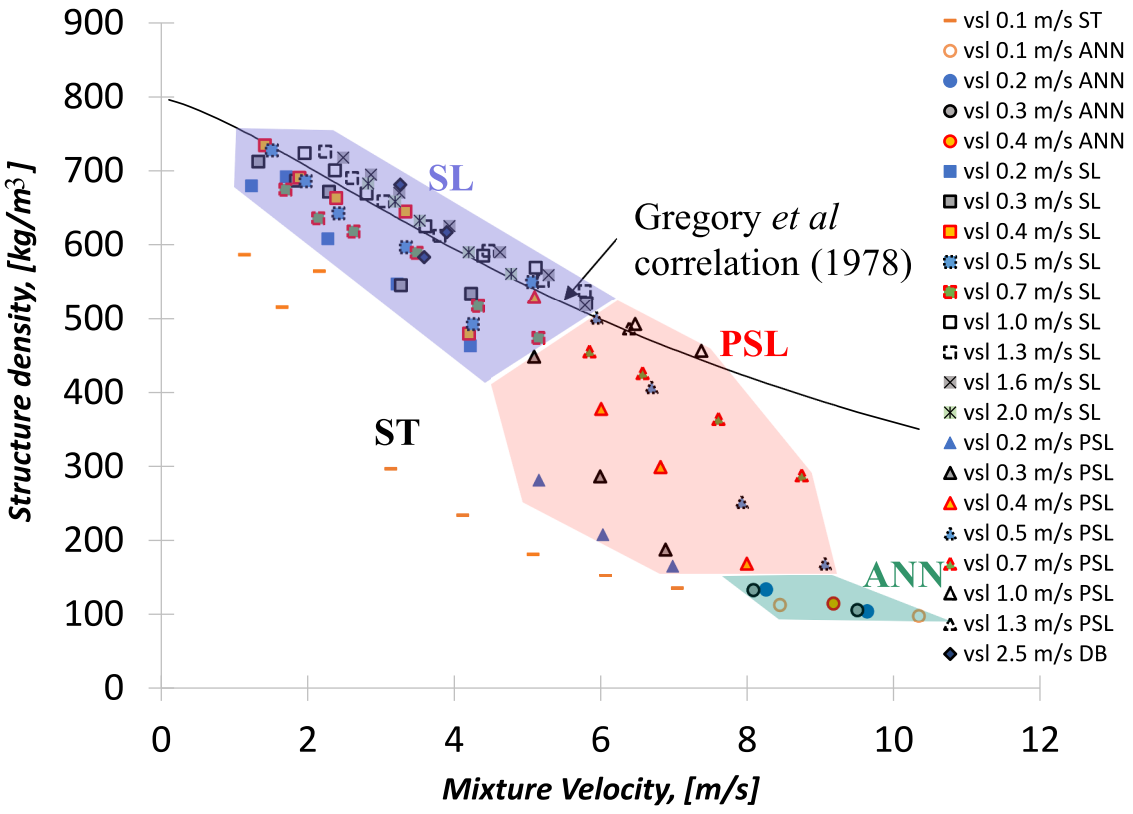

Fig. 7. Fluid-structure density (ρ_s).

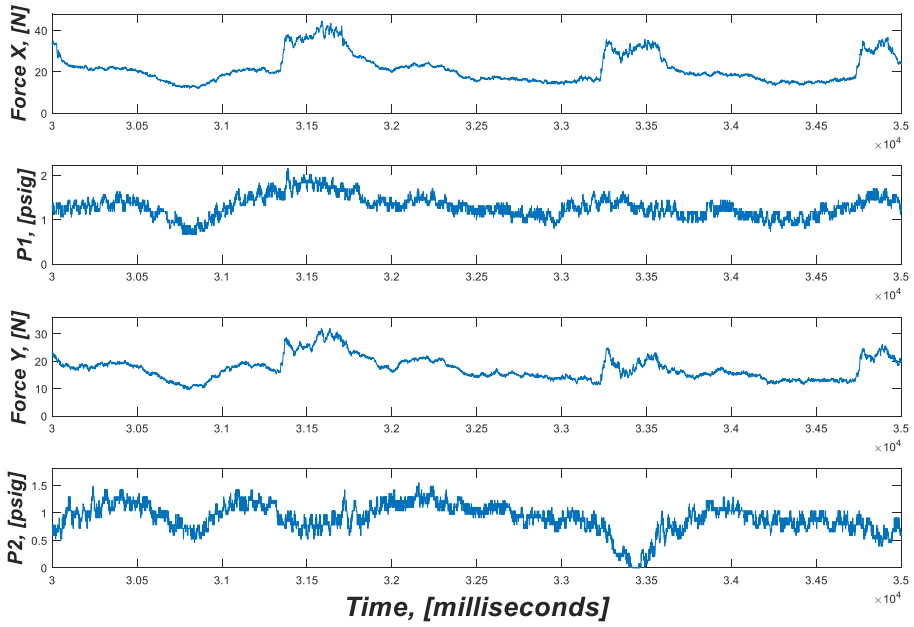

Fig. 8. Sample of flow force monitoring (slug, $v_{SL} = 0.70$, $v_{SG} = 1.93$ m/s).

elbow in a gas-liquid system. As v_{SG} increases, there are shorter waves of lower density (low average holdup, H_{LM}) and more pronounced peak forces. Although the structure density decreases as v_{SG} increases, the peak force increases due to the dominant effect of the structure velocity in the hydrodynamic force term.

The influence of the film region over the hydrodynamic force seems minimal, with values close to zero and independent of the liquid holdup fraction. Conversely, the flow and hitting of slug/pseudo-slugs cause the force peaks. Therefore, the force magnitude could be associated with the influence of the maximum values of momentum flux ($\rho_s v_T^2$).

Fig. 14 shows the hydrodynamic force evaluations for all the experimental repetitions. The data point values represent the mean for the repetitions, and the error bars its standard deviation. For $v_{SL} > 0.3$ m/s, there is more variation in the measured force. For some liquid levels, there are maximum values of hydrodynamic force as a function of mixture velocity (v_M). Fig. 14 also shows the results of the flow pattern

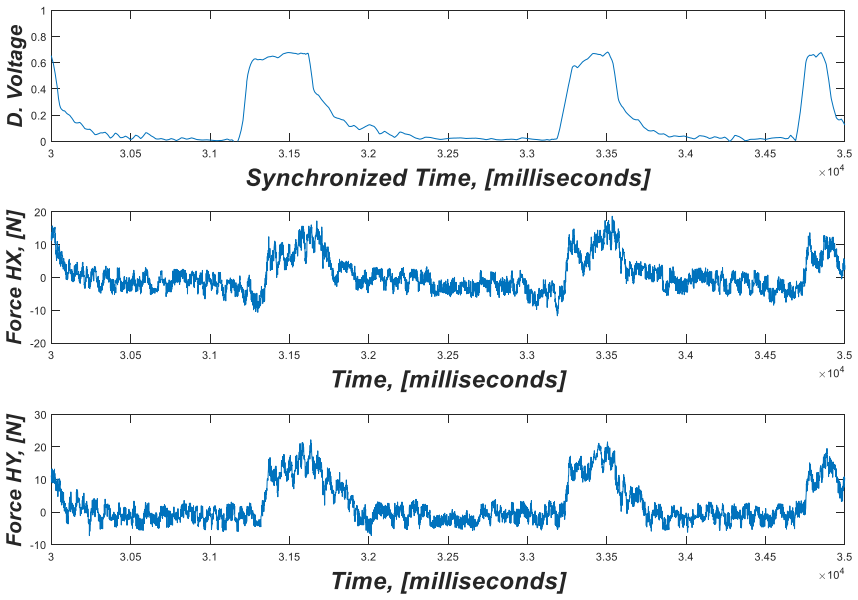

Fig. 9. Hydrodynamic Force (slug, $v_T = 3.65$ m/s, $\rho_s = 617.8$ kg/m3, $H_{LM} = 0.36$).

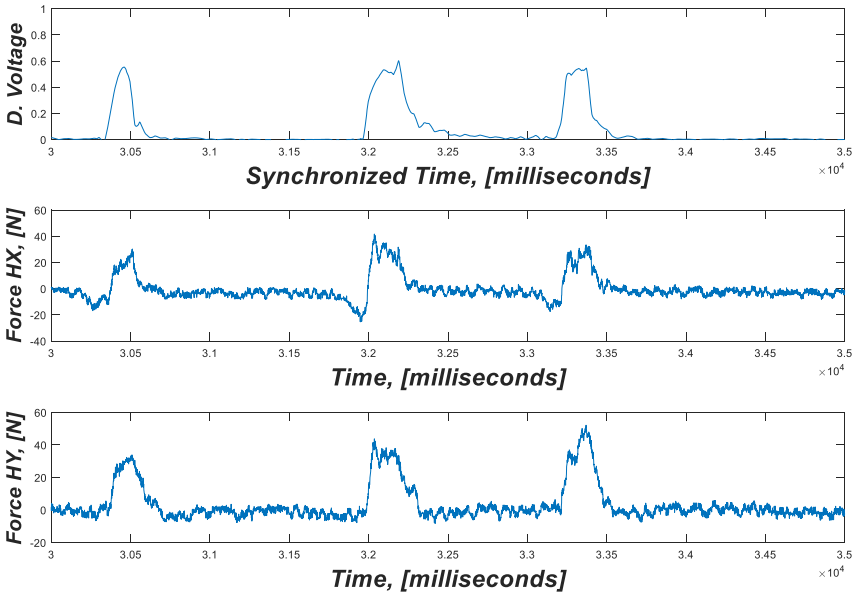

Fig. 10. Hydrodynamic force (slug, $v_T = 5.44$ m/s, $\rho_s = 518.1$ kg/m3, $H_{LM} = 0.28$).

characterization using the evaluation of the slug/pseudo-slug/wave hydrodynamic force.

The more pronounced structural vibration caused by the hydrodynamic force occurs in pseudo-slug flow (PSL), the transition from slug flow (SL) to annular flow (ANN), with high flow velocity and moderate structure density. For liquid superficial velocities v_{SL}>0.4 m/s, the hydrodynamic force reaches maximum values around 6 to 8 m/s of mixture velocity (v_M) in the PSL region. This observation agrees with the findings of Yih and Griffith (1968), which mentioned that the maximum fluctuations occur in the transition between the slug and annular flows. Fig. 15 shows the calculated maximum momentum flux ($\rho_s v_T^2 A$) vs. the maximum hydrodynamic force (F_H, percentile 97.5) extracted from measurements for all the flow conditions.

The comparison between the calculated momentum flux and measured hydrodynamic force shows a fair prediction, mainly for slug flow conditions. But it can be found that for pseudo-slug and annular wavy, parts of the relative errors exceed 20%. Those conditions maintain high force values on the elbow, regardless if they have less density and relatively less velocity (consequently less momentum flux) than the slug flow patterns. This could be explained by a possible impact force between the fluid structures of the liquid phase and the elbow (Liu et al., 2012), and the influence of high fluctuations in pressure.

Finally, the X and Y-axis force-time signatures were processed to get the main frequencies of the peak forces. Force frequency estimation was done using power spectra density (PSD) and discrete Fourier transformation (DFT) in the step of signal processing (see Fig. 4). The intermittent flow frequency (excitation) could be similar to peak-force frequency (reaction), depending on structural pipe parameters such as the damping coefficient (Kaneko et al. 2008). The system has recurrent frequencies above 60 Hz, identified using DFT for oil flow tests. Those could be related to the system's natural frequencies, and the excitation frequency is expected to be much lower without causing resonance in the system.

For the system evaluated, the flow frequency matches the

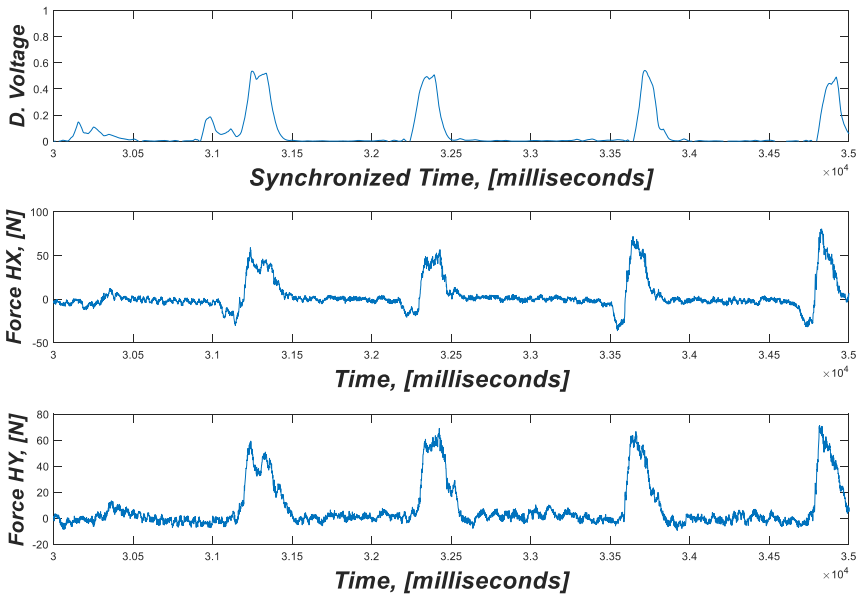

Fig. 11. Hydrodynamic force (pseudo-slug, $v_T = 6.73$ m/s, $\rho_s = 455.7$ kg/m3, $H_{LM} = 0.25$).

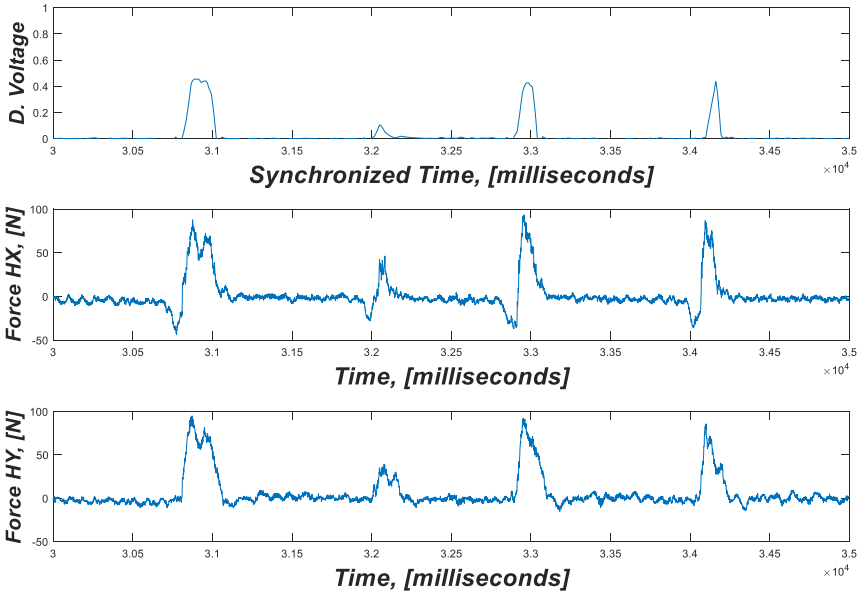

Fig. 12. Hydrodynamic force (pseudo-slug, $v_T = 8.24$ m/s, $\rho_s = 364.8$ kg/m3, $H_{LM} = 0.24$).

hydrodynamic force frequency means that there is a direct causal relationship between them, in which the cause is the flow behavior upstream of the pipe bend (see Fig. 16, first main DFT frequencies).

Since the force frequency follows the flow excitation, Fig. 17 shows the results of the flow pattern characterization using the evaluation of the slug/pseudo-slug/wave frequency. For lower gas rate in SL flow, frequency increases with increasing liquid fraction. For a given liquid superficial velocity, frequency changes slightly with increasing gas fraction for PSL and ANN. The flow conditions studied with frequency until 6 Hz could mean having flow stress cycles in the thousands or tens of thousands per hour, equivalent to millions of stress cycles per year.

3.2. Pressure fluctuation influence

The time signatures of flow and force were synchronized to understand better the influence of the unsteady flow on the resultant force. The expected hydrodynamic force contribution to the resultant force for a horizontal-horizontal 90° elbow would be:

$$\boldsymbol{F_{Hs}} = \boldsymbol{\rho_s v_T^2 A}\sqrt{2}. \tag{5}$$

Fig. 18 shows that the front of each slug is related to sudden increments of the resultant force acting on the elbow, generating peaks in the resultant force. However, the resultant force shows variations in the film region, which could be explained by the influence of pressure changes.

Figs. 19 and 20 show the resultant force and the pressure force on the elbow for two flow conditions, one for slug flow and one for pseudo-slug flow. The pressure force on the elbow would be equal to

$$\boldsymbol{F_P} = (\boldsymbol{P_E(t)A})\sqrt{2}, \tag{6}$$

assuming the pressure on the elbow $P_E(t)$ as the average between $P_1(t)$, and $P_2(t)$. As v_{SG} increases, the intensification of the amplitude of each peak force is caused mainly by increasing velocity, which dominates the

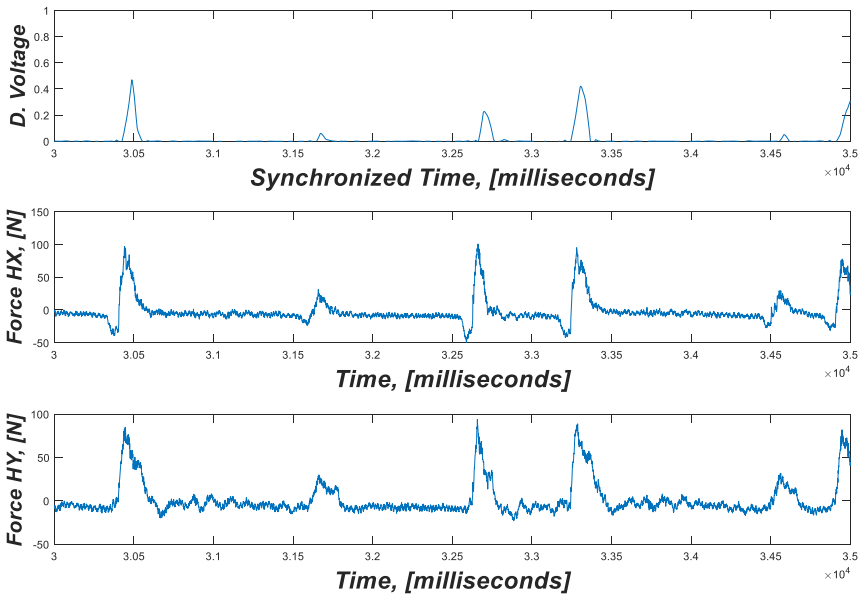

Fig. 13. Hydrodynamic force (pseudo-slug, $v_T = 8.81$ m/s, $\rho_s = 288.6$ kg/m3, $H_{LM} = 0.20$).

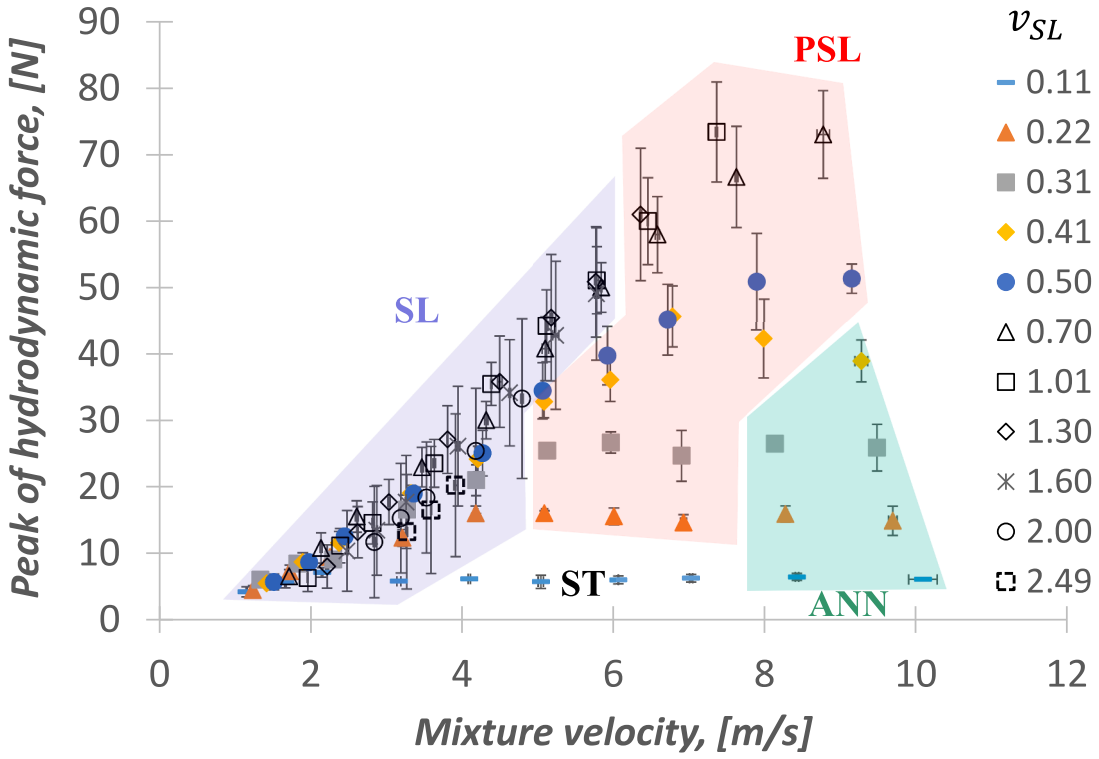

Fig. 14. Hydrodynamic force (F_H).

hydrodynamic force term.

The pressure force represents an essential component of the overall force, being almost the total force during the flow of the film region and contributing to the magnitude of the force peaks. In the peak force, the pressure changes from a low value to a high local value due to the arrival of each slug/pseudo-slug. Therefore, the force magnitude could include the hydrodynamic force and the pressure variation in this way:

$$F_{range} = F_{Hs} + \Delta F_P,$$
$$F_{range} = \left(\rho_s v_T^2 + \Delta P_E(t)\right) A\sqrt{2} \quad (7)$$

Thus, it is possible to include the pressure force effect using the difference between extreme percentiles as the P 97.5 and the P 2.5 (see example conditions in Table 2).

Therefore, as a general observation, there are time variations of force and pressure on the elbow in slug and pseudo-slug flow, characterized by sudden increases in pressure and the generation of hydrodynamic force peaks. Thus, the magnitude of the force peaks caused by the impact of intermittent flow on a horizontal-horizontal 90° elbow is reasonably predicted by including the influence of the momentum flux and variation of pressure force. See Fig. 21 for all the conditions that were studied. The comparison between the expected and measured force ranges shows a fair prediction (<20%), mainly for high flow force in pseudo-slug and

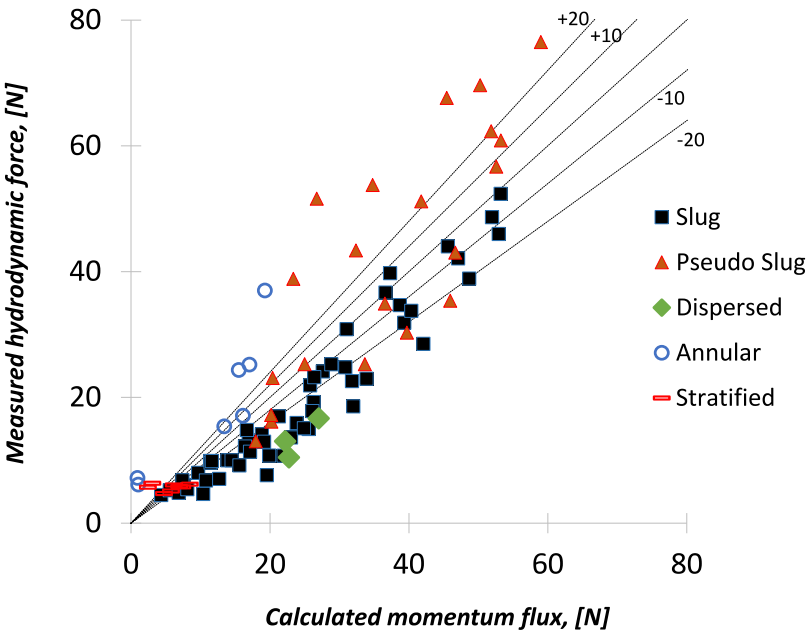

Fig. 15. Momentum flux ($\rho_s v_T^2 A$) vs. Hydrodynamic force (F_H, P 97.5).

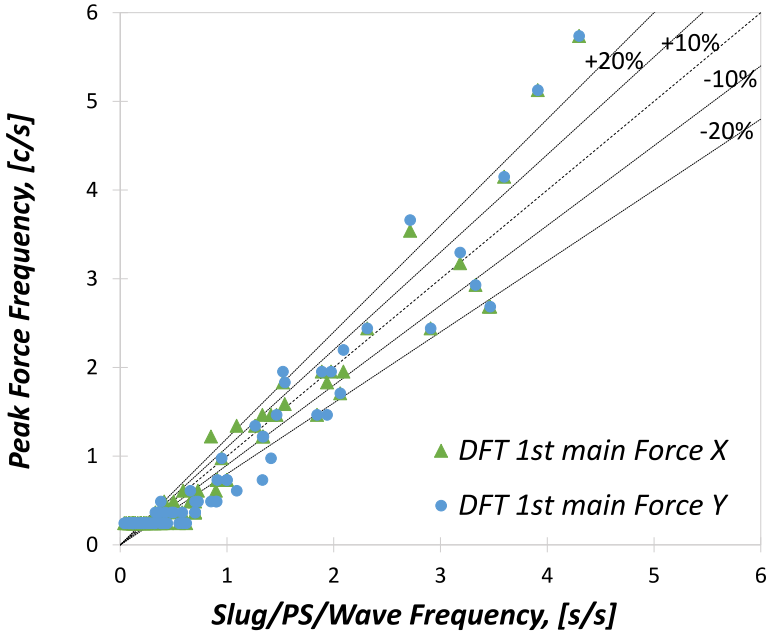

Fig. 16. Flow frequency vs. Peak-force frequency.

annular wavy conditions. Thus, pressure fluctuations in the elbow are significant for estimating the force in these flow patterns (PSL, ANN). Therefore, the multiphase variables required to be modeled besides fluid frequency are structure density, structure velocity, and pressure variation.

4. Concluding remarks

There are concluding remarks of the actual study related to the flow influence on the hydrodynamic force in a single elbow (90-degree) oriented in a horizontal-horizontal configuration. In terms of flow pattern, pseudo-slug flow led to more severe peak hydrodynamic forces, which resulted in more pronounced structural vibration. This happens during the transition from slug flow to annular flow, with high flow velocity and moderate structure density. For intermittent flow, the influence of film regions seems minimal, with values of hydrodynamic force close to zero independent of the liquid holdup fraction. Conversely, the flow and hitting of slug/pseudo-slugs are causing the force peaks. It is also interesting to observe that while pseudo-slug might be harmful due to its higher peak force, the slug flow is the flow pattern with the highest frequencies, which might accelerate the fatigue.

Now, in the case of the pressure effect, the pressure force could be seen as the base of the overall force, and its fluctuations influence not only the induced force during the flow of the film region but also contribute to the magnitude of the force peaks caused by the impact of flow structures. For this reason, the magnitude of the force peaks caused by the impact of intermittent flow on a horizontal-horizontal 90° elbow is reasonably predicted, including influences of momentum flux ($\rho_s v_T^2$),

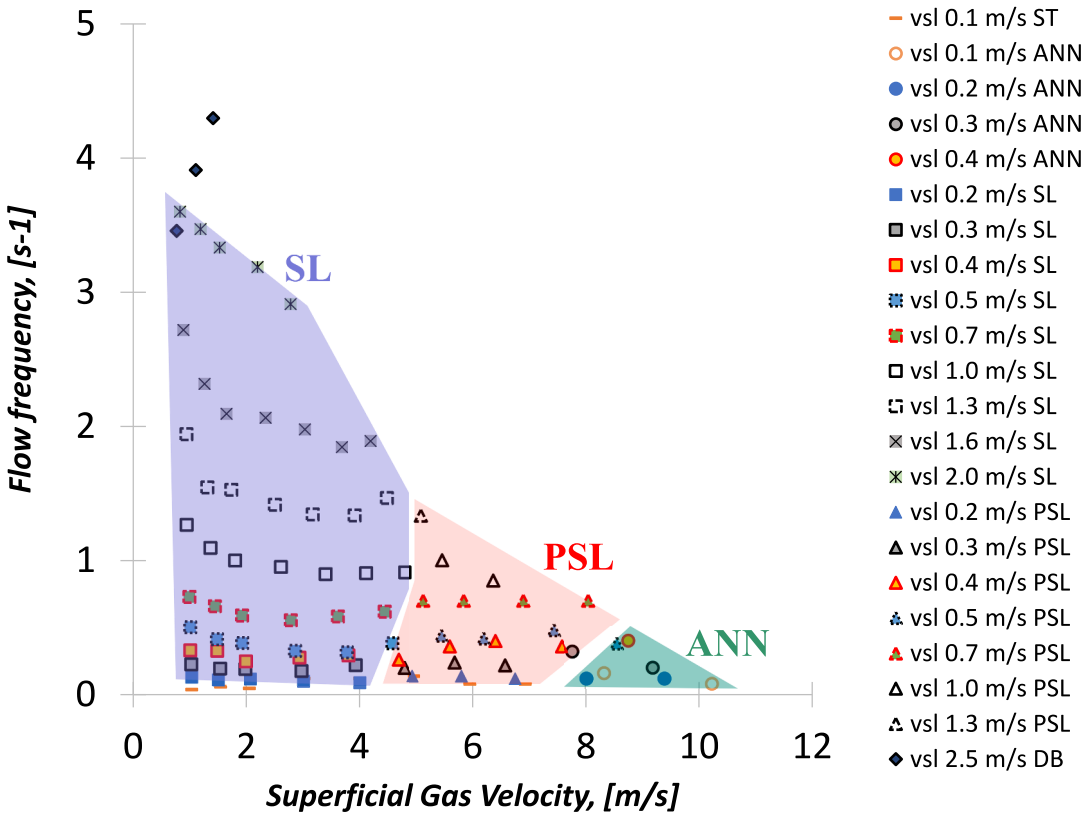

Fig. 17. Flow-structure frequency.

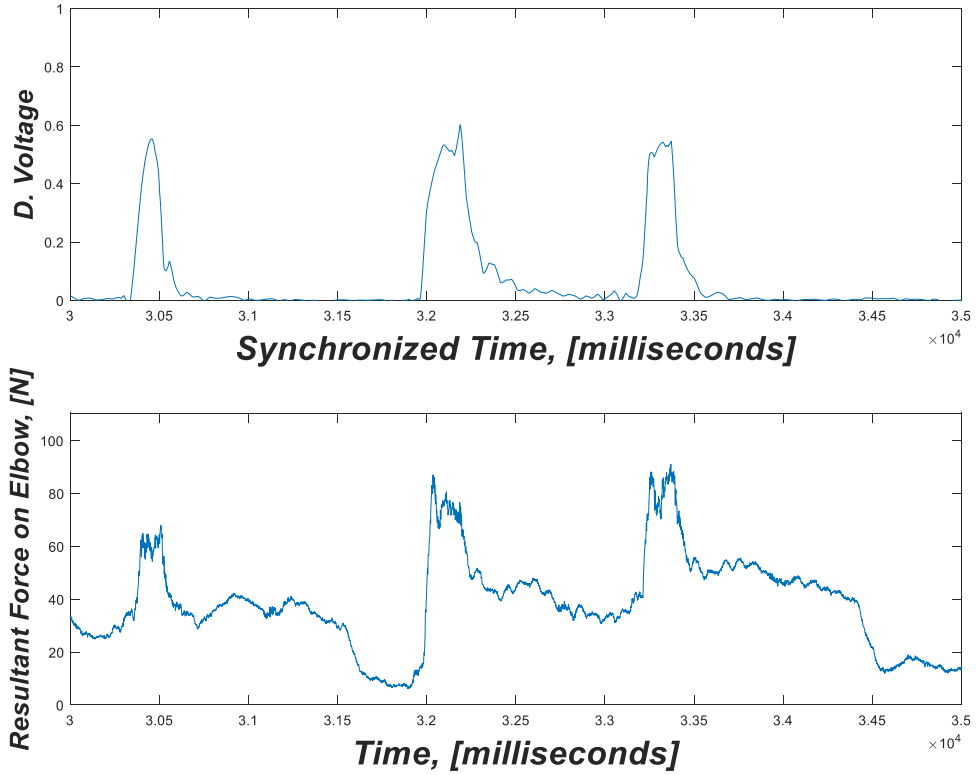

Fig. 18. Overall force (slug, $v_T = 5.44$ m/s, $\rho_s = 518.1$ kg/m3).

and variation of pressure force ($P_E(t)$).

Finally, for the system studied, the peak-force frequency is directly related to the flow-structure frequency upstream of the elbow. For lower gas rate in slug flow, frequency increases with increasing liquid fraction. For a given superficial liquid velocity, frequency changes slightly with increasing gas fraction for pseudo-slug and wavy annular. Therefore, the

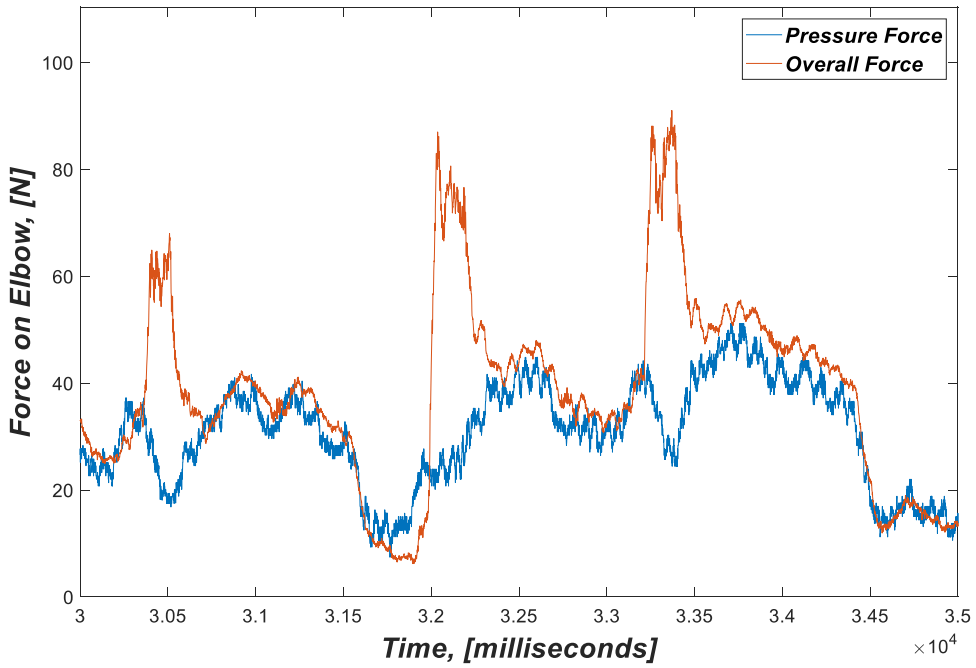

Fig. 19. Pressure force influence (slug, $v_T = 5.44$ m/s, $\rho_s = 518.1$ kg/m3).

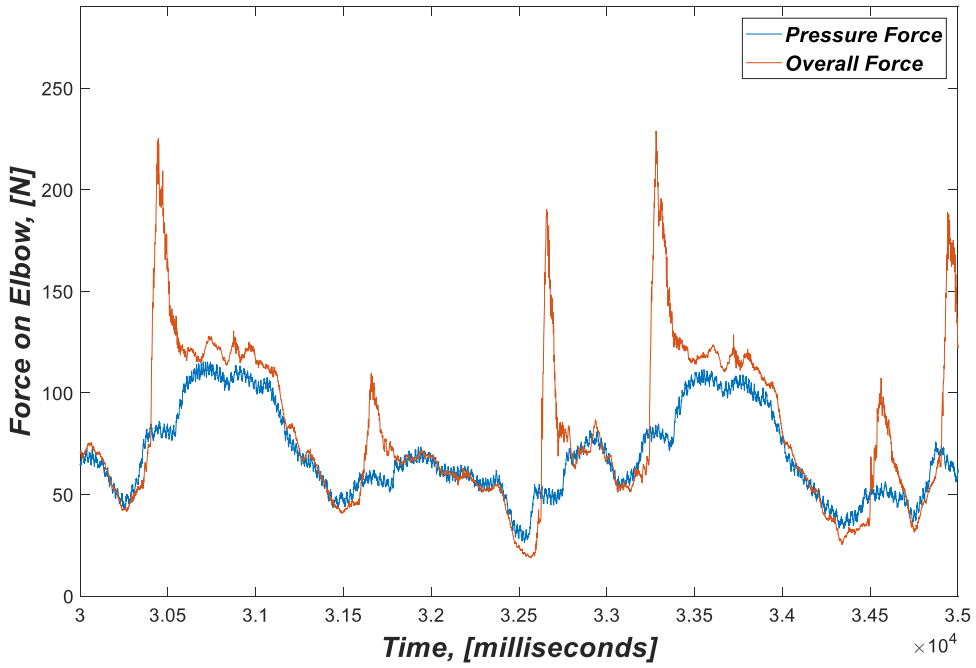

Fig. 20. Pressure force influence (pseudo-slug, $v_T = 8.81$ m/s, $\rho_s = 288.6$ kg/m3).

multiphase variables required to be modeled besides fluid frequency are structure density, structure velocity, and pressure variation.

CRediT authorship contribution statement

C. Garcia: Conceptualization, Methodology, Validation, Formal analysis, Investigation, Data curation, Writing – original draft, Visualization. **R. Nemoto:** Conceptualization, Methodology, Validation, Writing – review & editing. **E. Pereyra:** Project administration, Supervision, Writing – original draft, Resources, Formal analysis, Validation, Conceptualization. **L. Korelstein:** Validation, Writing – review & editing. **C. Sarica:** Funding acquisition, Resources, Supervision, Writing – review & editing, Conceptualization.

Declaration of Competing Interest

The authors declare that they have no known competing financial interests or personal relationships that could have appeared to influence the work reported in this paper.

Data availability

Data will be made available on request.

Table 2
Comparison of slug and pseudo-slug conditions.

Peak force magnitude	Slug (Fig. 19)	Pseudo-slug (Fig. 20)	Units
Lower pressure on the elbow (P 2.5)	0.60	1.37	psig
Higher pressure on the elbow (P 97.5)	2.59	5.83	psig
Flow structure velocity	5.44	8.81	m/s
Structure density	518.1	288.6	kg/ m^3
Expected hydrodynamic force, F_{Hs}	44.0	64.3	N
Expected pressure force, ΔF_P	19.6	88.4	N
Expected force magnitude, F_{range}	63.6	152.7	N
Measured force magnitude (P 97.5-P 2.5)	67.8	144.2	N

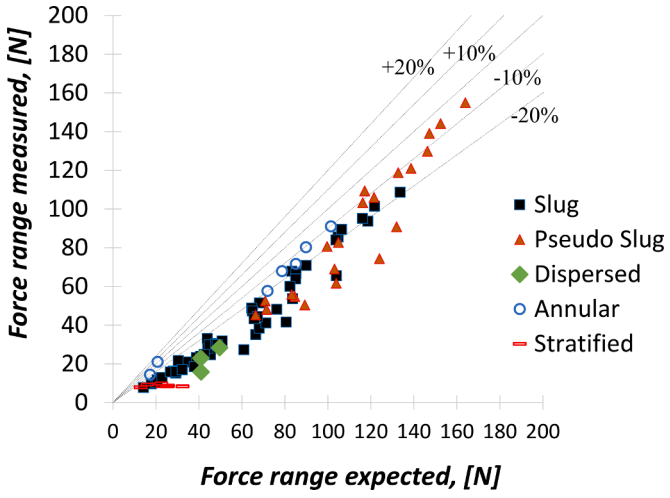

Fig. 21. Prediction of the magnitude of the force peaks (P97.5-P2.5).

Acknowledgments

Scott Graham (The University of Tulsa) and his team are acknowledged for their invaluable contributions to the experimental facility. TUFFP member companies are recognized for their suggestions during TUFFP Advisory Board meetings.

References

ASTM D341-09, 2015. Standard practice for viscosity-temperature charts for liquid petroleum products. ASTM Int. 125, 266–273 (2015).
Barnea, D., 1987. A unified model for predicting flow-pattern transitions for the whole range of pipe inclinations. Int. J. Multiph. Flow 13 (1), 1–12 (1987).
Belfroid, S.P.C., Schiferli, W., Cargnelutti, M.F., van Osch, M., 2010. Forces on bends and T-joints due to multiphase flow. In: Proceedings of the ASME 3rd Joint US-European Fluids Engineering Summer Meeting collocated with the 8th International Conference on Nanochannels, Microchannels, and Minichannels (2010).
Belfroid, S.P.C., Nennie, E., Lewis, M., 2016a. Multiphase forces on bend structures-influence of upstream disturbance. In: Proceedings of the 10th North American Conference on Multiphase Technology. Canada. BHR-2016-271 (2016).
Belfroid, S.P.C., Nennie, E., Lewis, M., 2016b. Multiphase forces on bends – large scale 6" experiments. In: Proceedings of the TNO and Xodus Group, SPE-181604-MS, SPE Annual Technical Conference and Exhibition held in Dubai, UAE, 26-28 September (2016).
Brito, R. (2012). "Effect of medium oil viscosity on two-phase oil-gas flow behavior in horizontal pipes." Thesis of Master of Science in Petroleum Engineering, The University of Tulsa, The Graduate School (2012).
BS 7608:2014+A1:2015, 2015. Guide to Fatigue and Assessment of Steel Products. Standard by British Standards Institution (BSI Group). Released December 31st (2015).
Cargnelutti, M.F., Belfroid, S.P.C., Schiferli, W., 2010. Two-phase flow-induced forces on bends in small scale tubes. J. Pressure Vessel Technol. 132. August 2010(2010).
Dieck, R.H., 2007. Measurement Uncertainty: Methods and Applications, 4th ed. ISA, The Instrumentation, System, and Automation Society, Printed USA. (2007).
DNV-05-F101, 2013. Submarine Pipeline Systems. Offshore standard, Det Norske Veritas AS. October (2013).
Gottfried, B.S., 1965. A mathematical model of thermal oil recovery in linear systems. In: Proceedings of the Society of Petroleum Engineers Jornal, SPE 1117, SPE Production Research Symposium held in Tulsa. OK. May 3-4 (1965.
Gregory, G.A., Nicholson, M.K., Aziz, K., 1978. Correlation of the liquid volume fraction in the slug for horizontal gas-liquid slug flow. Int. J. Multiph. Flow 4, 33–39 printed in Great Britain (1978).
Kaneko, S., Nakamura, T., Inada, F., Kato, M., 2008. Flow-induced vibrations classifications and lessons from practical experiences. Technical Section on Flow-Induced Vibrations JSME DMC Division, 1st ed. Elsevier, pp. 145–160. Chapter 4 Vibrations Induced by Internal Fluid flow(2008).
Liu, Y., Miwa, S., Hibiki, T., Ishii, M., Morita, H., Kondoh, Y., Tanimoto, K., 2012. Experimental study of internal two-phase flow induced fluctuating force on a 90° elbow. Chem. Eng. Sci. 76, 173–187 v2012.
Ortiz-Vidal, L.E., Mureithi, N.W., Rodriguez, O.M.H., 2017. Vibration response of a pipe subjected to two-phase flow: analytical formulations and experiments. Nucl. Eng. Des. 313, 214–224, 2017.
Riverin, J.L., de Langre, E., Pettigrew, M.J., 2006. Fluctuating forces caused by internal two-phase flow on bends. J. Sound Vib. 298, 1088–1098, 2006.
Riverin, J.L., Pettigrew, M.J., 2007. Vibration excitation forces due to two-phase flow in piping elements. J. Pressure Vessel Technol. 192, 7–13, 2007.
Shoham, O., 2006. Mechanistic Modeling of Gas-Liquid Two-Phase Flow in Pipes. SPE Book, Society of Petroleum Engineers, printed in the USA, 2006.
Soedarmo, A., Pereyra, E., Sarica, C., 2018. A simplified model for steady-state pseudo-slug flow. In: Proceedings of the Offshore Technology Conference, OTC-28996-MS, Paper Prepared for OTC Held in Houston. Texas, USA. April 30th – May 3rd (2018).
Tay, B.L., Thorpe, R.B., 2004. Effects of liquid physical properties on the forces acting on a pipe bend in gas-liquid slug flow. Chem. Eng. Res. Des. 82 (A3), 344–356. Trans. IChemE, Part A, March 2004.
Wang, L., Yang, Y., Li, Y., Wang, Y., 2018. Dynamic behaviours of horizontal gas-liquid pipes subjected to hydrodynamic slug flow: modeling and experiments. Int. J. Press. Vessels Pip. 161, 50–57, 2018.
Yih, T.S., Griffith, P., 1968. Unsteady Momentum Fluxes in Two-Phase Flow and the Vibration of Nuclear Reactor Components. Department of Mechanical Engineering, MIT, Cambridge, Massachusetts.
Zhang, H., Wang, Q., Sarica, C., Brill, J.P., 2003. Unified model for gas-liquid pipe flow via slug dynamics – Part 1: model development". J. Energy Res. Technol. 125, 266–273 (2018).